Reaction Chemistry & Engineering

ROYAL SOCIETY OF CHEMISTRY

PAPER

View Article Online
View Journal

Cite this: DOI: 10.1039/d5re00531k

Advanced capillary sampling technique for spatially resolved analysis of complex gas mixtures

Lisa Nordhausen, [a] Marie Denise Gutsch, [a] Daniel Hodonj [b] and Marion Börnhorst *[a]

Received 3rd December 2025,
Accepted 30th April 2026

DOI: 10.1039/d5re00531k

rsc.li/reaction-engineering

To investigate the spatial distribution of gas-phase species within structured catalysts under conditions representative of real exhaust gas environments, an invasive capillary-based sampling method was adapted for use in a hot gas test rig. A Fourier-transform infrared (FTIR) spectrometer was employed for analysis of gas mixtures characteristic for the selective catalytic reduction (SCR) of NO_x. To meet the sample volume requirements of the FTIR, a coil-based sampling extension was introduced and its influence was systematically quantified. A linear correlation between gas composition measurements with and without the coil enabled the development of a correction factor, which was generalized using a residence time model, thereby eliminating the need for extensive recalibration under different operating conditions. In addition, the impact of the capillary on local conversion behavior was assessed using an analytical model, accounting for uncertainties in capillary positioning and reduced gas velocities. These findings facilitated reliable spatially resolved species measurements for NH_3-SCR reactions. Extension of the methodology to a SCR configuration including the injection of urea water solution revealed significant challenges for a precise quantification of the gas composition due to transient phenomena such as film evaporation and deposit formation.

Introduction

Structured catalysts featuring small flow channels—such as honeycomb monoliths—are widely employed in various catalytic processes due to their favorable characteristics, including low pressure drop and high thermal conductivity. Accurate measurement of the reaction kinetics within the structured catalyst is essential for the development of predictive models describing reaction and transport processes, which represent the basis for efficient catalyst development. However, the small channel dimensions pose significant challenges for the spatially resolved measurement of temperature and gas-phase composition.[1] Notably, even within these confined geometries, non-uniform concentration profiles can develop along and across the channel axes, influencing the overall catalyst performance.[2]

For this purpose, the SpaciMS technology was developed, which enables spatially resolved measurements of concentrations in individual channels of a honeycomb catalyst with the use of a capillary.[3] While the capillary is sequentially moved along the channel axis, a mass spectrometer (MS) analyzes the sample composition, which requires comparatively small sample volumes for frequent analysis and therefore allows for online-monitoring of the intracatalytic concentrations.[3] In parallel, a thermocouple is inserted and moved within the channel with identical protocol. This technology enables in-operando spatially resolved concentration and temperature measurements, bridging integral and differential analysis of reaction kinetics. However, as a physical probe (capillary) is inserted to one or more catalyst channels, the SpaciMS technology is invasive. Previous works have investigated and quantified this influence using analytical models, computational fluid dynamics (CFD) simulations as well as experiments.[4–7] The flow disturbance of the sampling capillary within the catalyst channel is highly dependent on its radial position. When positioned at the center of the channel, the capillary induces the greatest perturbation to the flow field, whereas placement near the channel corner results in minimal flow field disruption. However, the exact radial position of the capillary cannot be accurately determined during the experiments, introducing a source of uncertainty.[5]

SpaciMS was used to investigate different exhaust gas aftertreatment systems such as diesel oxidation catalysts,[8,9] three-way-catalysts[10,11] and the selective catalytic reduction (SCR) of nitrogen oxides (NO_x).[12,13] In the context of SCR, challenges arise due to the superposition of the molar masses

[a] Institute of Reaction Engineering and Catalysis, TU Dortmund University, Emil-Figge-Straße 66, 44227 Dortmund, Germany.
E-mail: marion.boernhorst@tu-dortmund.de
[b] Institute for Chemical Technology and Polymer Chemistry (ITCP), Karlsruhe Institute of Technology (KIT), Engesserstraße 20, 76131 Karlsruhe, Germany

of H_2O and NH_3. This was described by Luo *et al.*[14] and Hou *et al.*[15] proposing to use a Fourier transform infrared spectrometer (FTIR) as analyzer instead of a MS. The SpaciFTIR technology enables the analysis of more complex gas mixtures, making it particularly valuable for studies related to Fischer–Tropsch synthesis[16] and ammonia oxidation.[17] Additionally, it provides important insights into SCR technologies in both conventional diesel engines and future hydrogen-powered engines.[18,19] However, in contrast to the MS, an FTIR requires a significantly larger sample volume. While this cannot be achieved through the capillary, Lou *et al.*[14,20] propose a dilution of the capillary sample with N_2. The required degree of dilution depends on the ratio of the capillary volumetric flow rate to the inert gas flow rate. For low capillary flow rates as considered in this study, high degrees of dilution would be required, which reduce the sensitivity of the FTIR measurements, thereby decreasing accuracy and limiting the detection of trace-level species. The low capillary flow rate is attributed to the use of a thin capillary, which minimizes flow distortion but leads to a low volumetric flow rate due to the high pressure drop across the capillary.

The present study applies the SpaciFTIR technology to the example of the SCR of NO_x. This technology is used for NO_x emission control of, *e.g.*, diesel engines, which are harmful to both the environment and health. Using NH_3 as reducing agent, NO_x are reduced following one of three reactions, depending on the NO/NO_x ratio:

$$4\ NO + 4\ NH_3 + O_2 \rightarrow 4\ N_2 + 6\ H_2O \quad (R1)$$

$$NO + 2\ NH_3 + NO_2 \rightarrow N_2 + 3\ H_2O \quad (R2)$$

$$8\ NH_3 + 6\ NO_2 \rightarrow 7\ N_2 + 12\ H_2O \quad (R3)$$

However, as ammonia is toxic, urea water solution (UWS) is used as a precursor in mobile applications. Known as AdBlue in Europe or DEF in the US, the solution contains 32.5 wt% urea dissolved in water. During the injection of liquid UWS, droplet–wall interactions lead to the formation of liquid films on the surfaces within the exhaust tract.[21,22] Within these films, isocyanic acid (HNCO), which is highly reactive in the liquid phase,[23] can accumulate and undergo undesired side reactions, resulting in the formation of solid deposits (*e.g.*, urea, biuret, cyanuric acid).[24,25] These deposits negatively impact the efficiency of NO_x reduction, as they reduce the effective generation of NH_3 and decompose slowly. Furthermore, the presence of liquid films and deposits complicates the precise control of UWS dosing, increasing the risk of under- or overdosing and thereby reducing system robustness and reliability.[26]

The targeted conversion of urea to ammonia takes place in two steps. The first step is the urea ($CO(NH_2)_2$) thermolysis, which produces NH_3 and isocyanic acid (HNCO). This is followed by the hydrolysis of HNCO, which produces NH_3 and CO_2:[27]

$$CO(NH_2)_2 \rightarrow NH_3 + HNCO \quad (R4)$$

$$HNCO + H_2O \rightarrow NH_3 + CO_2 \quad (R5)$$

The thermolysis of urea is generally assumed to occur upstream of the catalyst, primarily driven by thermal decomposition in the gas phase. However, due to the short residence times and the limited temperature in the exhaust system, complete decomposition of urea prior to the catalyst is often not achieved.[28] The resulting HNCO, formed as an intermediate, exhibits considerable thermal stability in the gas phase, necessitating the use of a catalyst to promote its hydrolysis to NH_3.[28] While dedicated hydrolysis catalysts can promote this conversion, employing SCR catalysts with integrated hydrolytic functionality provides a more practical and operationally efficient approach. The hydrolytic activity of commonly used SCR catalysts has been investigated for vanadia-based (V_2O_5/WO_3/TiO_2) formulations,[29] copper-exchanged zeolites (Cu-zeolites),[30] and iron-exchanged zeolites (Fe-zeolites),[31] each supported on monolithic substrates. These studies demonstrate that all aforementioned catalyst types exhibit catalytic activity toward the hydrolysis of isocyanic acid in addition to their primary NO_x reduction function. In the present work, a vanadia-based catalyst is employed, owing to its dual functionality in SCR and hydrolysis under relevant exhaust gas conditions.

Although the urea-SCR has been representing the state-of-the-art technology for NO_x abatement in mobile applications for two decades, the requirements of modern combustion engines and the ever stricter regulations and standards (Euro 7, US Tier 3)[32,33] demand for even higher efficiencies. Concepts aimed at reducing engine-out NO_x emissions, such as exhaust gas recirculation (EGR) or the intentional lowering of combustion temperatures, effectively decrease NO_x formation during the combustion process. However, these methods result in reduced exhaust gas temperatures, which adversely affect the urea thermolysis and HNCO hydrolysis. This, in turn, delays ammonia generation and slows down the reaction kinetics within the SCR catalyst. Close-coupled SCR systems, positioned near the engine, benefit from faster heat-up times and higher exhaust temperatures during cold-start and low-load operation. However, they introduce new challenges, particularly due to the shortened mixing length between UWS injection and catalyst inlet. This can lead to spatially non-uniform ammonia distribution in the exhaust stream, thereby reducing NO_x conversion.[24,34] For the optimization and targeted design of future exhaust gas aftertreatment systems, enabling improved efficiency and robustness under dynamic operating conditions, detailed insight into the simultaneous reaction kinetics of urea decomposition and NO_x reduction over the SCR catalyst is essential. As the majority of studies on SCR use gaseous NH_3 as the reductant rather than dosing urea, there is still limited information available on urea decomposition in combination with SCR reactions. SpaciFTIR enables spatially resolved analysis of the reaction progress and enables a deeper understanding of the thermolysis of urea, the subsequent catalytic hydrolysis of HNCO and the SCR reactions.

This study introduces a novel coil-based sampling configuration coupled with SpaciFTIR technology. A

methodological framework is developed and generalized on the example of NH_3-SCR, explicitly accounting for systematic measurement errors. The approach is subsequently applied to the urea-SCR system, providing first insights into the simultaneous reactions of urea-derived byproducts and NO_x over SCR catalysts through spatially resolved kinetic data.

Experiments

The following section outlines the experimental setup, followed by a description of the experimental procedures. Subsequently, the procedures for evaluating the measurement data are presented.

Hot gas test rig

The measurements are carried out in a hot gas test rig including a commercial AdBlue dosing unit for the investigation of multiphase reactions of urea decomposition and ammonia SCR, which is described in detail in our previous works on deposit formation[22,24] and spatially resolved measurements in the catalyst.[12] A schematic drawing is shown in Fig. 1. Given the primary focus on sampling and analysis, the remaining components of the system are not discussed in detail.

The synthetic exhaust gas flows into the injection section at a flow rate of approximately 1000 l min^{-1} and a gas temperature of approximately 280 °C. UWS is injected with a mass flow rate of 0.877 g min^{-1} and a pressure of 5 bar. This is accomplished through pulsed dosing at a frequency of 1 Hz with a duty cycle of 1%. Immediately downstream the urea injection zone, a 150 mm long commercial vanadia-based SCR catalyst (Umicore) is installed. It features a 600 cpsi honeycomb structure and a cross-sectional area of 30 × 60 mm. For reference measurements, a 120 mm long uncoated (catalytically inactive) honeycomb monolith with identical cell density and cross-sectional area is employed to investigate non-catalytic effects. To enable spatially resolved gas phase mole fraction measurements within the catalyst, a deactivated fused silica capillary is inserted into a single channel of the honeycomb monolith. Unless otherwise specified, the capillary is inserted to a channel in the top third of the monolith. The capillary is mounted on a motorized linear translation stage (OptoSigma), allowing precise axial positioning for spatially resolved sampling. The extracted gas is analyzed using an FTIR spectrometer (MultiGas 2030, MKS Instruments) to determine the local mole fractions of NH_3, NO, and CO_2 along the axial length of the catalyst. These species are selected to facilitate the investigation of urea thermolysis, HNCO hydrolysis, and the SCR reactions. As HNCO cannot be detected with spatial resolution due to a low signal-to-noise-ratio, CO_2 is used as a marker for hydrolysis progress, given its stoichiometric formation during the HNCO hydrolysis. Due to the low volumetric flow rate through the capillary of approximately 0.002 l min^{-1}, direct FTIR analysis in a sample chamber of 0.2 l would yield poor temporal resolution and increase the risk of cross-contamination. To mitigate these limitations, a coil-based configuration, analogous to that described by Tomin *et al.*,[35] is employed. The sample is pumped from the capillary through a 6-way valve using a vacuum membrane pump (KNF). The 6-way valve connects the pump conveying the sampled gas from the capillary, the exhaust exit, the purge gas (N_2), the coil, and the FTIR analytical system. In addition, it allows the coil to be operated with flow in both directions. Depending on the valve circuit, the sample flows either into the sample coil (V = 10 mL) ("load") or into the exhaust ("sample"). The two valve circuits are shown in Fig. 2. After filling the coil with the sample, it is purged with nitrogen and the gas sample is directed to the FTIR. In addition, the mole fraction upstream and downstream the catalyst is measured directly with the FTIR, without using the coil setup. These measurements, referred to as global measurements, represent the flow duct-averaged mole fractions upstream and downstream the catalyst and allow for the additional quantification of species that cannot be spatially resolved due to their low mole fractions, such as HNCO and NO_2. The upstream global mole fraction is sampled from the cover plate region, which may introduce inaccuracies due to potential liquid film formation and deposit accumulation upstream the catalyst. In contrast, the downstream global sampling is conducted in the outlet pipe,

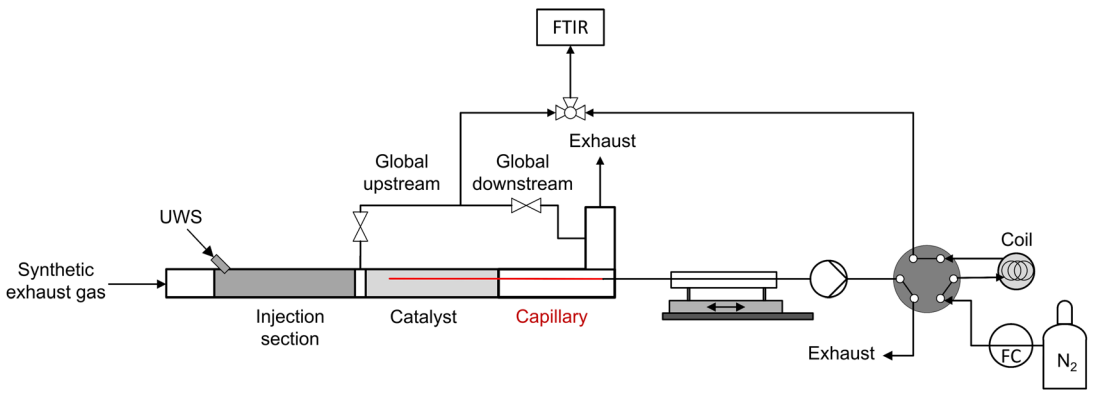

Fig. 1 Schematic of the hot gas test rig setup.

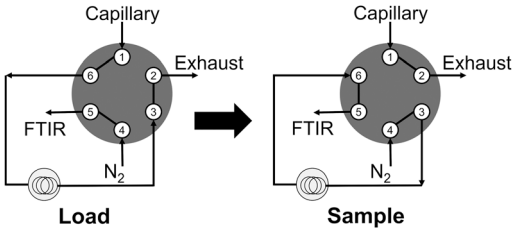

Fig. 2 Valve circuits of the 6-way valve.

where a more homogeneous gas-phase mixture can be assumed due to enhanced mixing conditions.

Three distinct experimental configurations are employed in this study:

1. Coil characterization tests using NH_3, NO, H_2, and CH_4 with an uncoated monolith,
2. Steady-state spatially resolved measurements of the NH_3-SCR over the catalyst and the uncoated monolith,
3. Spatially resolved measurements with UWS dosing over the catalyst, conducted with and without NO dosing.

The following sections provide a detailed description of the three experimental configurations.

Coil characterization tests

In the coil characterization experiments, the sampling behavior of the coil system is systematically evaluated, with particular focus on determining the optimal sampling time and quantifying the influence of the coil setup on measured species mole fractions. Initially, two different capillary inner diameters —150 μm ("thick") and 100 μm ("thin")—are compared to assess their impact on residence time and signal response. Subsequently, NH_3, NO, H_2, and CH_4 are dosed individually to flow through an uncoated honeycomb monolith under steady-state conditions to characterize the system response in the absence of reactions. For each gaseous species, a series of measurements is conducted at varying sampling durations, and the resulting coil mole fractions are compared with the corresponding global mole fractions upstream and downstream the catalyst. This procedure allows for a quantitative assessment of the relationship between global and coil mole fractions, forming the basis for a correction methodology applied in subsequent spatially resolved measurements. For hydrogen measurements, a hydrogen mass spectrometer (HSense, MS4 Analysentechnik) was used in addition to the FTIR.

Steady-state spatially resolved measurements of the NH_3-SCR

In these experiments, simultaneous dosing of NH_3 and NO is performed first over the uncoated honeycomb monolith to establish a non-reactive baseline, and subsequently over the SCR monolith to capture the reactive behavior. This sequential approach enables the highest spatial resolution in assessing the impact of the capillary and sampling system on the mole fraction measurements. The experimental procedure corresponds to that outlined below for the tests involving UWS dosing, with the exception that ammonia is supplied in gaseous form rather than being introduced *via* UWS injection.

Spatially resolved measurements with UWS dosing

The UWS dosing experiments are designed to investigate the simultaneous conversion of urea and NO, namely urea thermolysis, HNCO hydrolysis, and the SCR reaction pathway, under close-to-reality conditions in a spatially resolved manner.

Prior to the spatially resolved measurements, the sampling capillary is inserted into the catalyst from the downstream side. During the experiment, it is incrementally translated in flow direction, enabling axial profiling of the gas composition within the catalyst channel. At each axial position, three replicate measurements are performed to ensure reproducibility.

Each measurement cycle of the spatially resolved measurements consists of three steps:

1. Gas sampling for a duration of 6 minutes to fill the sampling coil (valve circuit: "load"),
2. Sample transfer to the FTIR system for a duration of 1 minute (valve circuit: "sample"),
3. Rinsing of the sampling coil with nitrogen for 3 minutes to prevent cross-contamination between measurements (valve circuit: "sample").

As a result, each measurement point requires approximately 30 minutes, including sampling, transfer, and purging cycles. Following each axial displacement of the capillary, a waiting period of 10 minutes was implemented to ensure that operation conditions were re-established prior to data acquisition. During this waiting period, the global gas composition was additionally measured to monitor the integral progress of urea thermolysis and HNCO hydrolysis. To achieve reproducible conditions during the measurement, the system is allowed to stabilize for 30 minutes after gas dosing begins and for 60 to 90 minutes following the initiation of UWS injection before the first measurement is taken.

Quantification of gas composition

The absorption peaks obtained from the FTIR spectra are integrated to determine the gas composition mole fractions by eqn (1).

$$y_{i,\mathrm{coil}} = \frac{T_{\mathrm{coil}}}{T_{\mathrm{purge}}} \cdot \frac{\dot{V}_{\mathrm{N2}}}{V_{\mathrm{coil}}} \cdot \int_{t_{\mathrm{peak,start}}}^{t_{\mathrm{peak,end}}} y_i(t)\,\mathrm{d}t \tag{1}$$

$$\int_{t_{\mathrm{peak,start}}}^{t_{\mathrm{peak,end}}} y_i(t)\,\mathrm{d}t = \sum_{j=1}^{N_{\mathrm{meas}}} \frac{y_{i,j} + y_{i,j+1}}{2} \cdot \Delta t_j - A_{\mathrm{cor}} \tag{2}$$

Here, $y_{i,\mathrm{coil}}$ denotes the species mole fraction of species i within the sampling coil, T_{coil} the temperature inside the coil, T_{purge} the temperature of the nitrogen purge gas and t the time. The variables $\dot{V}_{\mathrm{N2}}$ and V_{coil} represent the volumetric flow rate of the purge gas and the internal volume of the coil, respectively. The parameters $t_{\mathrm{peak,start}}$ and $t_{\mathrm{peak,end}}$ define the temporal bounds of the peak, y_i is the measured mole fraction and N_{meas} the number of data points used in the integration of the peak

signal. The corresponding integral used to quantify the species amount is discretized and evaluated *via* a rectangular (midpoint) numerical approximation, as illustrated in eqn (2). An empirical correction factor A_{cor} is introduced to account for potential deviations due to calibration uncertainties or signal drift. The correction area is computed as the average mole fraction over the final 50 data points preceding the peak signal.

The FTIR analysis results reflect the mole fractions present in the coil and cannot be directly interpreted as gas composition present in the catalyst channel. Because the analysis is influenced by residence time distribution effects, the measured mole fractions must be corrected to accurately represent the actual mole fraction at the sampling location. The quantification of the influence of the coil setup and a corresponding correction method are described in the results section.

Furthermore, the capillary intrusion affects the measurement results. Hlavatý *et al.*[6] demonstrated that the flow distortion of the capillary can be compensated through appropriate adjustment of the sampling flow rate. However, under the gas velocities and capillary dimensions (inner diameter 150 μm, outer diameter 375 μm) employed in the present study, such flow balancing is technically not feasible. To ensure accurate spatially resolved measurements the authors recommend to sample approximately 50% of the local channel flow rate through the capillary. Achieving this sampling fraction under the applied conditions would require a capillary flow rate of approximately 0.3 l min^{-1}, resulting in an unacceptably high pressure drop. Potential alternatives, such as employing a monolith with lower cell density (*e.g.*, 200 cpsi) or reducing the total volumetric flow rate, can increase the relative sampling fraction. However, these modifications would significantly alter the flow and thermal boundary conditions, thus compromising the representativeness of the exhaust gas conditions that the test rig is intended to replicate. Consequently, the approach presented by Hettel *et al.*[5] is adopted. The proposed model enables the quantitative assessment of capillary-induced residence time distortions as a function of the axial insertion depth, by incorporating both geometric parameters (*e.g.*, channel and capillary diameters) and operating conditions (*e.g.*, gas velocity).

Results and discussion

The measurement errors induced by the coil setup and the capillary intrusion are systematically analyzed and quantified in the following. The general procedure of data postprocessing and correction of systematic errors is presented in Fig. 3. The proposed methodology is applied for spatially resolved investigations of the NH_3-SCR and urea-SCR.

Influence of the coil

The influence of the sampling coil was evaluated based on the results of the coil characterization experiments. Mole fractions measured using two capillaries of different inner

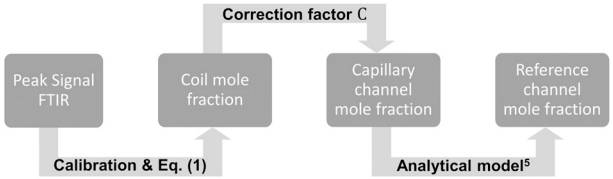

Fig. 3 Schematic of the data post processing.

diameters are compared with the corresponding global values across a range of sampling times. In addition, the hydrodynamic residence time (τ) within the coil is determined for both capillary configurations. The smaller capillary diameter leads to a reduction in flow field disturbance within the honeycomb structure, thereby yielding more representative spatial profiles.[5] However, this benefit comes at the cost of a reduced volumetric flow rate, which limits the sensitivity and speed of gas sampling. As illustrated in Fig. 4, the mole fraction stabilizes for sampling times exceeding the hydrodynamic residence time in the case of the thicker capillary. However, the mole fraction measured without the coil setup (global) is not reached. With the thinner capillary, the mole fraction exhibits a clear dependence on the sampling time. Even after 20 minutes, the ratio of the coil mole fraction to the global mole fraction remains below 0.5. The higher hydrodynamic residence time in the coil observed for the thinner capillary is attributed to the reduced volumetric flow rate in the thinner capillary under identical pressure drop conditions. Additionally, axial dispersion effects become more pronounced in the thinner capillary due to the lower flow velocity and smaller cross-section, which leads to increased peak broadening and reduced temporal resolution. As a result, the thinner capillary was excluded from further use. Furthermore, the sampling time was set to 6 min for the thicker capillary, as this corresponds to the best trade-off between accuracy and experimental duration.

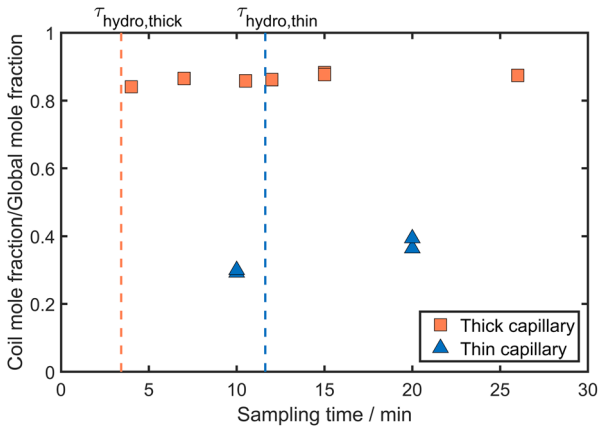

Fig. 4 Comparison of the ratio of the coil mole fraction and global mole fraction using a thick (ID 150 μm) and a thin (ID 100 μm) capillary over different sampling times.

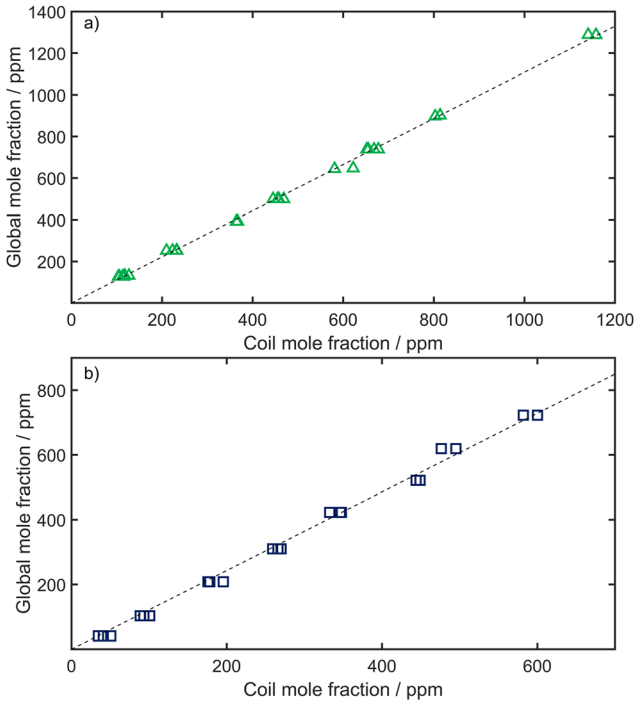

Fig. 5 Measured global mole fractions over coil mole fractions of a) NO and b) NH_3. $\dot{V}_g$ = 1000 l min^{-1}, $T_{g,in}$ = 25 °C.

For a detailed quantification of the deviations of the measured coil mole fractions from the actual global value, the respective mole fractions for the two main components of SCR, NH_3 and NO, are measured and compared for a concentration range relevant to SCR as shown in Fig. 5. A linear correlation is observed for both components, indicating that the relationship between the coil-derived and global mole fractions is independent from the absolute concentration levels. To quantify this relationship, a linear regression was applied to the data points, constrained to pass through the origin. This constraint is physically justified, as in the absence of dosing, the corresponding mole fraction must be zero. The resulting regression line thus provides a consistent basis for correcting coil measurements across varying concentrations.

Based on the linear regression, a correction factor (C) is introduced which corresponds to the slope of the respective function and is defined as the ratio of the coil mole fraction and the global mole fraction ($y_{i,\mathrm{global}}$) of component i:

$$C = \frac{y_{i,\mathrm{coil}}}{y_{i,\mathrm{global}}} \tag{3}$$

$$y_{i,\mathrm{cor}} = \frac{y_{i,\mathrm{coil}}}{\mathrm{C}} \tag{4}$$

The correction factor is required to relate the measured coil mole fraction to the actual probed channel mole fraction ($y_{i,\mathrm{cor}}$). It primarily depends on the local sampling volume flow, which in turn is influenced by the total volumetric flow rate, the gas temperature, as well as the radial and axial position of the sampling capillary within the monolith channel.

Due to the high experimental effort and the need to repeat this procedure for each operating condition, an analytical model for the correction factor is applied. This model is based on the residence time sum function, which describes the cumulative probability that a fluid element introduced at the reactor inlet at time t = 0 will exit the system within a time interval [0, t]. Given that the Reynolds number in the coil remains below 1 (Re < 1), laminar tube flow conditions are assumed in the coil. Accordingly, a laminar flow residence time distribution (RTD) model is applied. Furthermore, axial dispersion is considered negligible, as the Bodenstein number satisfies Bo ≫ 100 for all investigated gas species, indicating minimal backmixing and validating the laminar tubular flow approximation. This results in the following relationship for the hydrodynamic residence time:[36]

$$\tau = \frac{L}{\overline{u}} = \frac{\pi \cdot R^2 \cdot L}{\dot{V}} = \frac{\pi \cdot R^2 \cdot u(r) \cdot t}{\dot{V}} \tag{5}$$

$$\left(\frac{r}{R}\right)^2 = 1 - \frac{\tau}{2t} \tag{6}$$

$$F(t) = \begin{cases} 1 - \frac{1}{4}\left(\frac{\tau}{t}\right)^2, & \text{for } t \geq \frac{\tau}{2} \\ 0, & \text{for } t < \frac{\tau}{2} \end{cases} \tag{7}$$

Let R and L denote the radius and length of the coil, respectively, $u(r)$ the velocity and r the radial coordinate. The hydrodynamic residence time τ is defined as the ratio of the coil volume to the volumetric flow rate through the capillary ($\dot{V}$). By substituting the analytical velocity profile for laminar flow in a cylindrical tube, the expression for τ can be reformulated (eqn (6)). This relationship is subsequently incorporated into the cumulative residence time distribution function, $F(t)$, yielding eqn (7).

Since the residence time sum function must remain positive for all t, eqn (7) is not valid for short times. Therefore, for $t < \frac{\tau}{2}$, an alternative expression is applied to ensure mathematical and physical consistency. This model allows for the analytical prediction of the residence time sum curve as a function of both elapsed time and sampling flow rate. Based on that, a theoretical coil mole fraction value is determined by establishing a time-discretized mole balance for the species (eqn (8)). Incorporating the ideal gas law, along with the definitions of mole fraction and concentration and under the assumption of constant inlet and outlet flow rates, leads to the expression given by eqn (9),

$$n_{i,\mathrm{coil}}(t + \Delta t) = n_{i,\ \mathrm{coil}}(t) + \dot{n}_{i,\mathrm{in}} - \dot{n}_{i,\mathrm{out}} \tag{8}$$

$$y_{i,\mathrm{coil}}(t + \Delta t) = y_{i,\mathrm{coil}}(t) - F(t) \cdot y_{i,\mathrm{in}} \cdot \frac{\dot{V}_{\mathrm{cap}}}{V_{\mathrm{coil}}} + y_{i,\mathrm{in}} \cdot \frac{\dot{V}_{\mathrm{cap}}}{V_{\mathrm{coil}}} \tag{9}$$

where $n_{i,\mathrm{coil}}$ denotes the molar amount of component i in the sample coil, $\dot{n}_{i,\mathrm{in}}$ and $\dot{n}_{i,\mathrm{out}}$ the inlet and outlet molar flow rate of component i and $\dot{V}_{\mathrm{cap}}$ the volume flow through the capillary. To validate the model, the theoretically calculated

correction factors are compared with experimentally determined values in Fig. 6 for different gas species. The black line represents the theoretically calculated correction factor, while the cross markers denote the corresponding experimentally determined values. The species investigated include NO and NH_3, both of which are directly relevant to SCR reaction mechanisms; H_2, which is of growing interest in the context of future hydrogen-fueled engines; and CH_4, an important reactant in various combustion and power-to-X applications. The comparison reveals that, particularly at short sampling durations, the model provides a sufficient representation of the experimental data for all species. For higher sampling times, the model exhibits a slight underestimation of the correction factor for NO, H_2, and CH_4, while the overall agreement remains satisfactory. A notable deviation is observed in the case of ammonia, for which the model consistently underpredicts the correction factor across all sampling intervals. This discrepancy is attributed to adsorption phenomena on the inner wall of the sampling coil,[32,33] as evidenced by the delayed desorption observed during the nitrogen purge phase, where NH_3 requires significantly longer flushing times to be fully displaced.

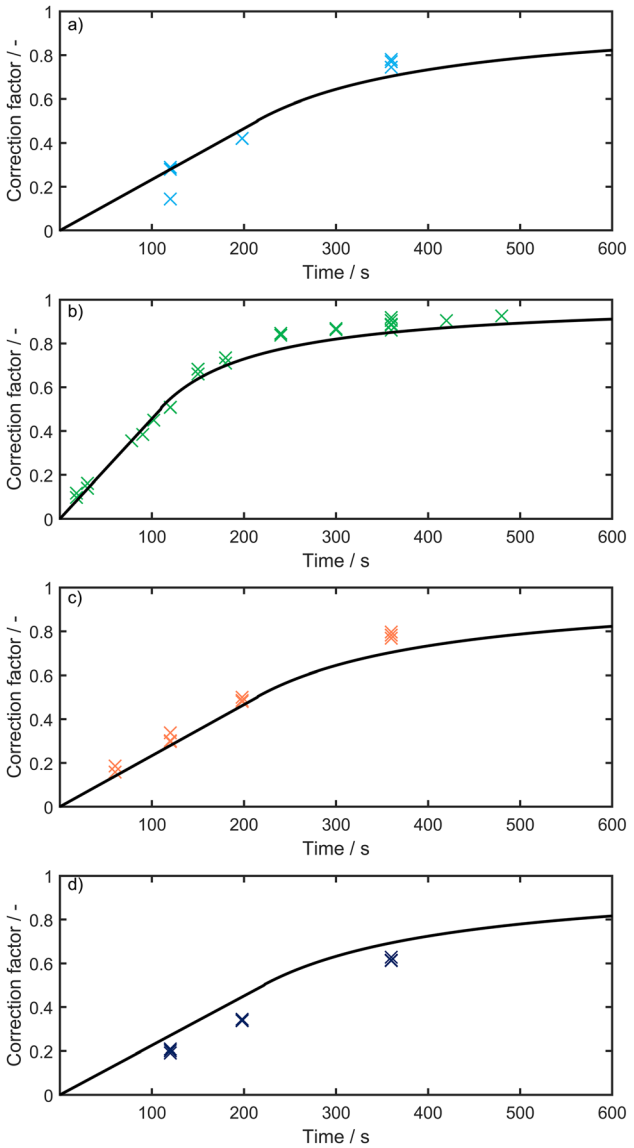

Fig. 6 Comparison of the modeled (black line) and the experimentally (crosses) determined correction factor over the sampling time for different species: a) H_2, b) NO, c) CH_4 and d) NH_3.

Influence of the capillary

The insertion of a capillary into a monolith channel reduces the effective cross-sectional area, increasing the pressure drop within the probed channel. As a result, the volumetric flow rate in the probed channel is lower than in an unprobed reference channel. This leads to an increased residence time in the probed channel and therefore to a higher conversion compared to unprobed channels.

The extent of this flow disturbance strongly depends on the axial and radial position of the capillary. For downstream insertion, as applied here, the influence increases as the capillary tip approaches the catalyst inlet. This can be explained by the total pressure drop consisting of contributions from the empty channel section and the capillary-containing section. Since the former is significantly smaller, extending the capillary further upstream increases the overall pressure drop. Due to the increased pressure drop, the volumetric flow rate through the probed channel decreases, leading to a reduction in flow velocity. As the capillary is moved further downstream, two opposing effects occur: the reduction in flow velocity becomes less pronounced, while the length, over which the reduced velocity increases the residence time, becomes larger.

In addition, most conversion occurs in the front section of the channel, where reactant concentrations are highest, further amplifying the impact of upstream placement. The effect of radial position is commonly evaluated using two limiting cases, as the exact radial position during operation is unknown: maximum flow perturbation for a centered capillary and minimum disturbance for placement near the corner region.[5,6]

As previously discussed, the influence of the sampling capillary is quantitatively evaluated in this study using the analytical model developed by Hettel *et al.*[5] The two limiting cases regarding the radial position are evaluated using the methodology of Gossler *et al.*[37] for determining the friction factor. For both limiting cases, the mole fractions in a reference channel, unaffected by capillary-induced flow disturbances, are calculated for each axial position, representing the minimum and maximum measurement deviation. These estimates are presented in Fig. 7 alongside the capillary channel mole fraction, corrected using the developed methodology, on the example of ammonia SCR. The black dashed lines and empty green triangles represent the estimated mole fraction within a reference channel, where the upper tip corresponds to capillary placement at the

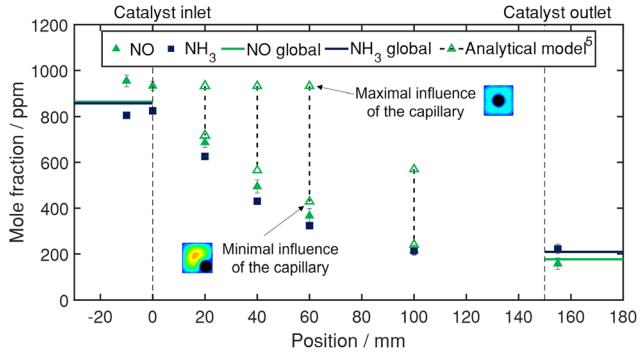

Fig. 7 Spatially resolved measurements of NO (filled green triangles), NO mole fraction in a reference channel (empty green triangles) and corresponding data for NH_3 (blue rectangles) and global measurements (lines) over a vanadia-based catalyst. The grey dotted lines mark the catalyst inlet and outlet. Black arrows indicate the potential influence of the capillary on the NO mole fraction. $\dot{V}_g$ = 1000 l min^{-1}, $T_{g,in}$ = 274 °C, $y_{NO,set}$ = 1000 ppm.

radial channel center (maximum flow distortion), and the lower tip to placement at the corner (minimum flow distortion). The reference channel mole fractions of NO are presented here as a representative example; however, the observed deviations are applicable to all detected species.[5]

An approximately equimolar decline in NO and NH_3 mole fractions is observed, consistent with the expected stoichiometry of the standard SCR reaction (eqn (R1)). As the axial shift along the catalyst increases, the concentration profiles of NH_3 and NO converge progressively. This behavior is partially attributed to the presence of small quantities of NO_2 (approximately 1% of the NO mole fraction), formed *via* equilibrium between NO and NO_2. NO_2 cannot be measured in spatially resolved manner due to its low concentrations.

Comparison with global measurements—conducted without the capillary setup—reveals that the mole fraction downstream the outlet of the capillary-probed channel equals the average across all channels. This demonstrates that the effect of the coil can be accurately accounted for using the correction factor. At the inlet, deviations—most pronounced for NO—can be attributed to turbulence effects upstream the honeycomb structure as well as slight variations in capillary positioning. The small error bars, derived from three-fold measurements at each point, demonstrate a high degree of reproducibility.

The influence of the capillary increases steadily over the first 60 mm, reaches a maximum at this position, and then decreases sharply. Although the flow distortion is greatest at a position of 10 mm as discussed previously, the impact on the mole fractions continues to increase up to 60 mm. This can be attributed to the fact that a longer upstream section with reduced velocity due to the capillary leads to a greater increase in residence time. It should be noted that the predicted mole fractions under conditions of maximum flow distortion are bounded by the inlet mole fractions to ensure physical consistency. However, the calculated values exceed the inlet mole fractions by up to 170 ppm. At 60 mm the initially high reaction rate, which decreases along the channel, coincides with the progressive residence time shift induced by the capillary. Beyond this point, the influence diminishes, as the overall reaction rate declines with decreasing reactant mole fractions and the mole fraction gradients become nearly uniform toward the channel outlet. Based on the observed data, it is inferred that the capillary is located close to the corner of the channel. This is evident from the observation that the values associated with the capillary effect align more closely with the global data when the capillary is positioned in the corner of the channel. For reasons of clarity, the influence of the capillary is not depicted in the following, as its precise radial position within the channel during the experiment is unknown, thereby impeding an exact quantification of its impact on the measured concentrations.

Spatially resolved measurements with UWS dosing

Fig. 8 presents spatially resolved species profiles obtained under conditions of UWS injection combined with gaseous NO dosing. In addition to NH_3 and NO, CO_2 mole fractions are measured, as the intermediate species HNCO cannot be detected with spatial resolution due to the low signal-to-noise ratio and the comparatively small peaks due to the sample coil. Consequently, HNCO hydrolysis is assessed indirectly *via* the corresponding change in CO_2 mole fraction. Furthermore, mole fractions of NO, NH_3, CO_2, and HNCO calculated using a one-dimensional plug-flow tubular reactor (1D PFTR) model are presented, with kinetic parameters estimated from the mole fraction profiles reported in this

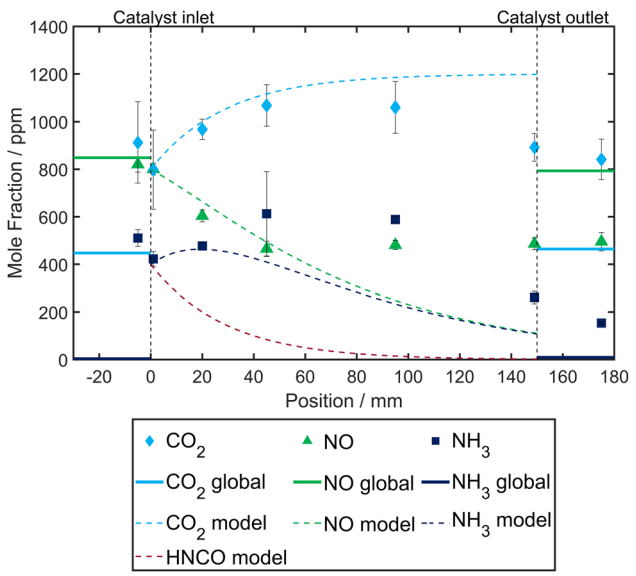

Fig. 8 Spatially resolved measurements of NO (green triangles), NH_3 (blue rectangles) and CO_2 (light blue diamonds) global measurements (solid lines) and modeled mole fractions (dashed lines) over a vanadia-based catalyst. The dotted lines show the catalyst inlet and outlet. $\dot{V}_g$ = 1140 l min^{-1}, $T_{g,in}$ = 277 °C, $y_{NO,set}$ = 900 ppm, $\dot{m}_{UWS}$ = 0.877 g min^{-1}.

study. The model results are intended to provide qualitative guidance on the expected trends (including HNCO) rather than quantitative predictions. For an accurate kinetic description, more detailed investigations on the catalytic HNCO hydrolysis are required, which are the subject of ongoing research.

Model predictions show a sharp decrease in HNCO mole fraction in the inlet section approaching zero at approximately 120 mm. The CO_2 mole fraction increases correspondingly, which can be attributed to HNCO hydrolysis. The predicted NO mole fraction decreases along the entire catalyst length due to the standard SCR reaction (eqn (R1)). The NH_3 mole fraction increases slightly near the inlet and then decreases. This results from the superposition of NH_3 production *via* HNCO hydrolysis and NH_3 consumption by the SCR reaction.

The measurement uncertainties presented in Fig. 8 are significantly larger than those observed in Fig. 7. This is primarily attributed to transient effects introduced by pulsed UWS injection. The presence of a liquid phase, along with film and deposit formation upstream the catalyst, results in a spatially and temporally non-uniform reactant distribution across the flow duct, which will be addressed in more detail below.

First, the spatially resolved data are discussed, followed by a comparison with the global data. The NH_3 mole fraction increases in the first section of the probed channel as a result of urea thermolysis and HNCO hydrolysis, and decreases toward the channel outlet due to the consumption of NH_3 in the standard SCR reaction with NO. Similarly, the CO_2 mole fraction rises within the first 45 mm of the channel, as expected from HNCO hydrolysis, and then stabilizes. This observation aligns with the expectation that HNCO hydrolysis predominantly occurs in the first half of the catalyst. However, the observed CO_2 mole fraction at the catalyst inlet (0 mm) is higher than anticipated based on stoichiometric considerations. Approximately 420 ppm CO_2 originate from the CO_2 content in the feed air, implying that roughly 400 ppm CO_2 is formed upstream of the catalyst. If this CO_2 formation results from HNCO hydrolysis, approximately 800 ppm NH_3 (400 ppm from urea thermolysis and 400 ppm from HNCO hydrolysis) would be expected upstream. However, measurements show only about 400 ppm NH_3 at the catalyst inlet. As the mole fractions at the channel inlet are used as model input, this discrepancy is not reflected in the model predictions.

Furthermore, an offset between mole fractions immediately upstream (−4 mm) of and at the catalyst inlet (0 mm) is observed, which is likely attributable to backmixing and turbulence effects induced by the cross-sectional contraction at the catalyst entrance.

Contrary to expectations and the model predictions, the NH_3 and NO mole fractions remain approximately constant throughout the second half of the catalyst. Despite the presence of both reactants, further SCR conversion appears to be negligible, suggesting a cessation or significant reduction of the reaction, which does not align with prior results. This can be attributed to the measurement protocol. It requires approximately 30 minutes per spatially resolved data point—comprising three repetitions of 6 minutes of gas sampling and 3 minutes of nitrogen purging—resulting in limited temporal resolution. Consequently, transient fluctuations, such as the entrainment of liquid droplets into the sampling capillary, may lead to local concentration spikes that are not adequately captured by the current approach. While good agreement between spatially resolved measurements and model predictions is observed in the upstream region, deviations increase toward the downstream section. This suggests that, with longer injection durations, the influence of film and deposit formation becomes more significant and cannot be adequately resolved. Additionally, simultaneous acquisition of global and spatially resolved data is not feasible as it would require the use of a second FTIR. As a result, temporal variations in the inlet gas composition cannot be tracked continuously, making it impossible to precisely correlate the inlet conditions with individual axial measurement positions.

In contrast to the spatially resolved measurements, lower conversions of NO are observed in the global measurements, which can be attributed to the increased residence time caused by flow distortion and associated stagnation upstream the capillary in the probed channel. Upstream the catalyst, approximately 450 ppm of CO_2 is detected globally, which can be attributed to ambient CO_2 present in the intake air. Measurement uncertainties for CO_2 are higher than for NH_3 and NO, primarily due to fluctuations in laboratory air composition, which affect the baseline CO_2 level. Moreover, almost no NH_3 is observed upstream the catalyst, suggesting that neither thermolysis nor HNCO hydrolysis occurs significantly upstream the catalyst. However, this observation may also be influenced by non-uniform NH_3 distribution within the exhaust duct. Due to the pressurized injection of UWS from the top and notable liquid film formation and deposit accumulation on the bottom wall, the NH_3 distribution is expected to be inhomogeneous.[38] The global sampling position at the top wall of the duct upstream the catalyst is assumed to diminish representative sampling. In contrast, downstream global measurements are taken from the well-mixed exhaust gas flow, providing a more representative composition. The global measurements reveal only a marginal increase in CO_2 mole fraction—approximately 30 ppm—accompanied by a significant NO slip of about 790 ppm. The measured global NH_3 mole fraction downstream the catalyst is approximately 10 ppm. The observed CO_2 increase implies that around 60 ppm of NH_3 was generated through thermolysis and subsequent HNCO hydrolysis, which is consistent with the simultaneous reduction of NO by approximately 55 ppm (global) and the measured NH_3 slip of 10 ppm. Experimental data and observations suggest that a substantial portion of the UWS forms solid deposits rather than undergoing the intended thermal decomposition and hydrolysis reactions to produce

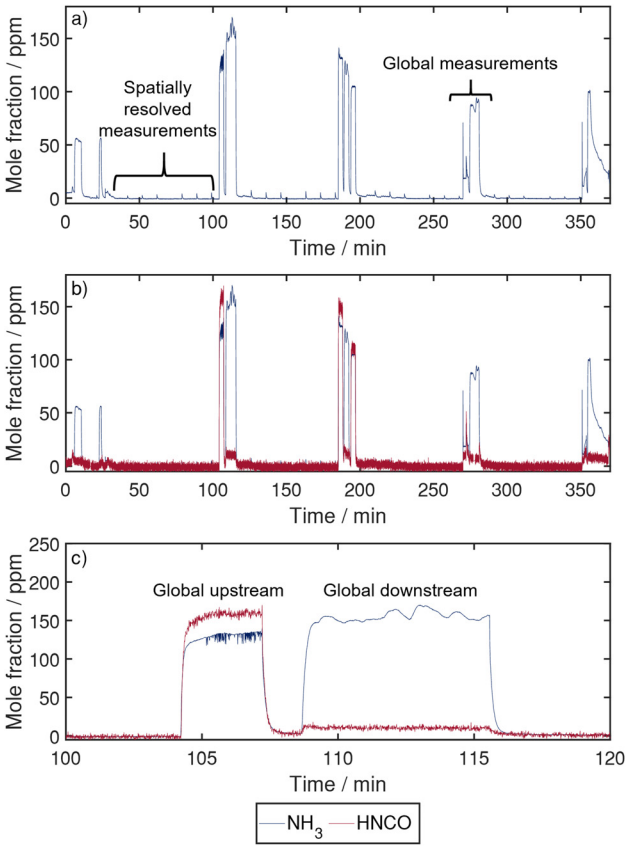

Fig. 9 Temporal evolution of global mole fraction profiles: a) time-dependent variation of NH_3 (blue), b) superimposed mole fraction profiles of NH_3 and HNCO (red), and c) enlarged view of the superimposed global NH_3–HNCO mole fraction profiles. $\dot{V}_g$ = 1000 l min^{-1}, $T_{g,in}$ = 280 °C, $\dot{m}_{UWS}$ = 0.877 g min^{-1}

NH_3. To enable a more detailed examination, the progression of the global data throughout the duration of the experiment is evaluated.

Fig. 9 presents the global mole fractions of NH_3 (blue) and HNCO (red) during an experiment conducted under identical operating conditions but without NO dosing. The prominent peaks correspond to the global measurements, while the smaller, superimposed peaks in the NH_3 signal reflect spatially resolved measurements. The global mole fractions exhibit significant temporal fluctuations. Initially, a continuous increase in both NH_3 and HNCO mole fraction is observed, followed by a gradual decline after a transitional point. This behavior can be attributed to the evaporation of the majority of the liquid film in the early phase of the experiment, promoting urea thermolysis. As the experiment progresses and the temperature of the bottom plate decreases due to pronounced film formation and the formation of solid decomposition products becomes more dominant, less NH_3 and HNCO are generated.

Closer inspection of the global data—exemplified by the measurement at 104 minutes in Fig. 9c—reveals that nearly identical mole fractions of NH_3 and HNCO are present upstream the catalyst. The slight deviation is attributed to non-uniform concentration distribution across the duct and the fixed sampling position. Downstream the catalyst, however, only a few ppm of HNCO is detected, indicating efficient hydrolysis. Ideally, the sum of the upstream NH_3 and HNCO mole fractions should correspond to the total amount detected downstream. The observed discrepancy reinforces the conclusion that incomplete mixing occurs upstream the catalyst, potentially affecting reaction efficiency and measurement accuracy.

To examine the non-uniform distribution of reactive species across the catalyst cross-section in detail, two experiments conducted under identical operating conditions within different measurement channels are compared in Fig. 10. In both cases, UWS was injected without the addition of NO to study urea thermolysis and HNCO hydrolysis. In the experiment labeled "top", the sampling capillary was positioned in a channel located in the upper third of the catalyst cross-section, whereas in the "bottom" experiment, it was placed in a channel in the lower third.

Significantly reduced NH_3 and CO_2 mole fractions were observed in the "top" experimental configuration. This is attributed to gravitational spray settling and film formation at the bottom of the duct, acting as a reservoir for decomposition products, as well as the 30° downward injection angle of the UWS, which increases the likelihood of droplet impingement and localized concentration peaks in the lower region of the catalyst. In the upper sampling area, the NH_3 mole fraction decreases over time, indicating a gradual reduction in the supply of HNCO and NH_3 upstream due to deposit formation.

In contrast, the "bottom" experiment reveals significantly higher NH_3 and CO_2 mole fractions. The initial increase in NH_3 mole fraction is consistent with the onset of HNCO hydrolysis, while the CO_2 mole fraction, which also initially increases as a product of hydrolysis, subsequently slightly decreases. This decline is likely attributable to factors such

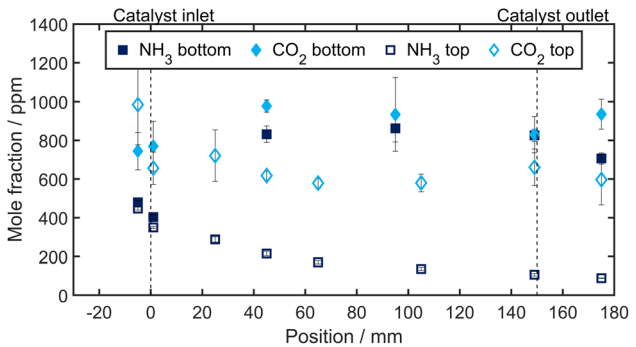

Fig. 10 Comparison of two spatially resolved measurements of NH_3 (blue squares) and CO_2 (light blue diamonds). The filled symbols represent data obtained with the capillary positioned in a channel located in the lower third of the catalyst cross-section, while the open symbols correspond to measurements taken from a channel in the upper third. Vertical dashed lines indicate the inlet and outlet boundaries of the catalyst. $\dot{V}_g$ = 1000 l min^{-1}, $T_{g,in}$ = 278 °C, $\dot{m}_{UWS}$ = 0.877 g min^{-1}.

as non-uniform reactant mixing, deposit formation and varying CO_2 inlet concentrations. This strongly suggests the occurrence of additional reactions within the liquid film, leading to a pronounced spatial dependence of the mole fraction profiles.

Furthermore, the data indicate that HNCO hydrolysis progresses significantly faster in the lower half of the catalyst. However, further investigation is required to determine whether these observations are the result of spatial variations or are influenced by temporal effects.

These findings underscore the pronounced impact of injection strategy and potential wall film formation on the spatial distribution of reactive species within the catalyst. The results demonstrate that a precise quantification of spatially resolved mole fractions with the proposed measurement technique is strongly impeded by the transient characteristics of UWS dosing and decomposition measurements. Static mixers potentially mitigate spatial concentration inhomogeneities, however, strong turbulence and flow distortion have to be accepted.

Conclusions

In the scope of this work, an invasive capillary-based sampling technique was adapted for application in a hot gas test rig operating under conditions representative of real exhaust systems. To reduce measurement inaccuracies arising from spectral overlap between NH_3 and H_2O, an FTIR spectrometer was employed. To meet the sample volume requirements of the FTIR, a customized coil setup was implemented. The influence of this configuration on the measurement accuracy was systematically characterized, revealing a linear correlation between data obtained with and without the coil. Based on this observation, a correction factor was introduced to compensate for the residence time effects introduced by the coil.

To further generalize this correction, a laminar tube flow-based residence time model was applied, enabling the calculation of the correction factor without the need for extensive calibration experiments under different operating conditions. This model was validated against experimental data for multiple gas species and showed good agreement, with the exception of ammonia. For NH_3, systematically lower mole fractions—and consequently underestimated correction factors—were observed. This deviation is attributed to adsorption effects on the inner surfaces of the coil, corroborated by the delayed desorption of NH_3 during nitrogen purging.

In addition, the influence of the capillary on local catalytic conversion was evaluated using an analytical model. As this model does not account for the gas volume removed through the capillary, it serves as the worst-case estimate for the measurement deviation induced by capillary intrusion. The primary sources of uncertainty in this context include the unknown radial position of the capillary within the channel cross-section and the high gas velocities, which amplify flow disturbances. To increase the accuracy of error estimation, a method for continuous position tracking during operation must be developed. Alternatively, the approach employed by Hlavatý *et al.*[6] to compensate for capillary-induced effects could be adopted. However, implementing such a method poses significant technical challenges under the experimental conditions applied in this study. Compared to the dilution method first proposed by Luo *et al.*,[14] the present approach is particularly suitable for low capillary volumetric flow rates. However, due to its increased experimental complexity and potential limitations in temporal resolution, the method proposed by Luo *et al.* may be preferable at higher capillary flow rates. The applicability and limitations of both methods depend on the analytical technique employed, the target species, and the corresponding detection limits.

Despite the limitations of the developed methodology, it enabled reliable acquisition of spatially resolved data for the NH_3-SCR reaction system. The approach was subsequently extended to the more complex urea-SCR reaction system. The obtained spatial mole fraction profiles partially deviated from expectations, largely due to the low temporal resolution of the measurement method and the transient nature of film and deposit formation during UWS dosing.

Based on these findings, adaptations to the experimental setup are recommended to improve measurement representativeness and reliability. The implementation of a static mixer in combination with optimized flow control can enhance the homogeneity of species distribution across the catalyst cross-section, thereby improving the spatial accuracy of global measurements.[39,40] Alternatively, an optimized UWS dosing strategy could be developed to reduce temporal fluctuations and approach steady-state conditions. Such improvements would be particularly valuable for laboratory-scale studies aiming to investigate urea thermolysis and HNCO hydrolysis under controlled conditions, supporting the development and optimization of SCR catalysts. Additionally, to capture transient effects with greater fidelity, alternative analytical techniques with higher temporal resolution, which in this case particularly requires a smaller sample volume, ideally circumventing spectral interference between NH_3 and H_2O, should be explored.

Author contributions

Lisa Nordhausen: conceptualization, methodology, formal analysis, investigation, writing – original draft, writing – review and editing, visualization. Marie Denise Gutsch: methodology, formal analysis, investigation. Daniel Hodonj: methodology, investigation. Marion Börnhorst: conceptualization, writing – review and editing, supervision, project administration, funding acquisition.

Conflicts of interest

There are no conflicts to declare.

Data availability

Data for this article, including the FTIR spectra of the spatially resolved measurements are available at TUDOdata, https://doi.org/10.17877/TUDODATA-2025-MIECVP6U.

Acknowledgements

The authors would like to thank the Deutsche Forschungsgemeinschaft (DFG - German Research Foundation) for their financial support within the Collaborative Research Centre CRC/TRR 150 "Turbulent, chemically reactive, multi-phase flows near walls", project number 237267381. Provision of the catalyst by Umicore is kindly acknowledged.

Notes and references

1 K. Morgan, J. Touitou, J.-S. Choi, C. Coney, C. Hardacre, J. A. Pihl, C. E. Stere, M.-Y. Kim, C. Stewart, A. Goguet and W. P. Partridge, Evolution and Enabling Capabilities of Spatially Resolved Techniques for the Characterization of Heterogeneously Catalyzed Reactions, *ACS Catal.*, 2016, **6**, 1356–1381.

2 J. Sá, D. L. A. Fernandes, F. Aiouache, A. Goguet, C. Hardacre, D. Lundie, W. Naeem, W. P. Partridge and C. Stere, SpaciMS: spatial and temporal operando resolution of reactions within catalytic monoliths, *Analyst*, 2010, **135**, 2260–2272.

3 W. P. Partridge, J. M. E. Storey, S. A. Lewis, R. W. Smithwick, G. L. Devault, M. J. Cunningham, N. W. Currier and T. M. Yonushonis, Time-Resolved Measurements of Emission Transients By Mass Spectrometry, *SAE Trans.*, 2000, 2983–2991.

4 M. Hettel, C. Diehm, B. Torkashvand and O. Deutschmann, Critical evaluation of in situ probe techniques for catalytic honeycomb monoliths, *Catal. Today*, 2013, **216**, 2–10.

5 M. Hettel, C. Antinori and O. Deutschmann, CFD Evaluation of In Situ Probe Techniques for Catalytic Honeycomb Monoliths, *Emiss. Control Sci. Technol.*, 2016, **2**, 188–203.

6 T. Hlavatý, P. Kočí, M. Isoz, D. Deka and W. Partridge, Balanced Fast-SpaciMS capillary configurations provide practically noninvasive channel-average measurements in catalytic monoliths, *Chem. Eng. Sci.*, 2023, **282**, 119272.

7 H. Nguyen, P. Y. Peng, D. Luss and M. P. Harold, Assessing intrusion by the capillary during spatially resolved mass spectrometry measurement, *Chem. Eng. J.*, 2017, **307**, 845–859.

8 A. Abedi, J.-Y. Luo and W. S. Epling, Improved CO, hydrocarbon and NO oxidation performance using zone-coated Pt-based catalysts, *Catal. Today*, 2013, **207**, 220–226.

9 D. Chan, S. Tischer, J. Heck, C. Diehm and O. Deutschmann, Correlation between catalytic activity and catalytic surface area of a Pt/Al2O3 DOC: An experimental and microkinetic modeling study, *Appl. Catal., B*, 2014, **156-157**, 153–165.

10 A. Lanza, D. Bounechada, S. Raphy, R. Sato, L. Phillipson, A. Kolpin and A. P. York, The effect of the oxygen storage material on a three-way catalyst spatio-temporally resolved with Spaci-MS, *Catal. Today*, 2024, **437**, 114775.

11 C. Coney, C. Hardacre, K. Morgan, N. Artioli, A. P. York, P. Millington, A. Kolpin and A. Goguet, Investigation of the oxygen storage capacity behaviour of three way catalysts using spatio-temporal analysis, *Appl. Catal., B*, 2019, **258**, 117918.

12 M. Eck, P. Lott, D. Schweigert, M. Börnhorst and O. Deutschmann, Spatially Resolved Measurements of HNCO Hydrolysis over SCR Catalysts, *Chem. Ing. Tech.*, 2022, **94**, 738–746.

13 C. Kuntz, P. J. Jägerfeld, J. Mmbaga, R. E. Hayes and O. Deutschmann, Coupling of Liquid and Surface Chemistry in Urea SCR Systems, *Emiss. Control Sci. Technol.*, 2023, **9**, 77–92.

14 J.-Y. Luo, X. Hou, P. Wijayakoon, S. J. Schmieg, W. Li and W. S. Epling, Spatially resolving SCR reactions over a Fe/zeolite catalyst, *Appl. Catal., B*, 2011, **102**, 110–119.

15 X. Hou, S. J. Schmieg, W. Li and W. S. Epling, NH3 pulsing adsorption and SCR reactions over a Cu-CHA SCR catalyst, *Catal. Today*, 2012, **197**, 9–17.

16 F. Kapteijn, R. M. de Deugd and J. A. Moulijn, Fischer–Tropsch synthesis using monolithic catalysts, *Catal. Today*, 2005, **105**, 350–356.

17 V. A. Sadykov, L. A. Isupova, I. A. Zolotarskii, L. N. Bobrova, A. S. Noskov, V. N. Parmon, E. A. Brushtein, T. V. Telyatnikova, V. I. Chernyshev and V. V. Lunin, Oxide catalysts for ammonia oxidation in nitric acid production: properties and perspectives, *Appl. Catal., A*, 2000, **204**(1), 59–87.

18 C. Özyalcin, S. Sterlepper, S. Roiser, H. Eichlseder and S. Pischinger, Exhaust gas aftertreatment to minimize NOX emissions from hydrogen-fueled internal combustion engines, *Appl. Energy*, 2024, **353**, 122045.

19 P. Lott, U. Wagner, T. Koch and O. Deutschmann, Der Wasserstoffmotor – Chancen und Herausforderungen auf dem Weg zu einer dekarbonisierten Mobilität, *Chem. Ing. Tech.*, 2022, **94**, 217–229.

20 J.-Y. Luo, H. Oh, C. Henry and W. Epling, Effect of C3H6 on selective catalytic reduction of NOx by NH3 over a Cu/zeolite catalyst: A mechanistic study, *Appl. Catal., B*, 2012, **123-124**, 296–305.

21 S. Grout, J.-B. Blaisot, K. Pajot and G. Osbat, Experimental investigation on the injection of an urea–water solution in hot air stream for the SCR application: Evaporation and spray/wall interaction, *Fuel*, 2013, **106**, 166–177.

22 M. Börnhorst, C. Kuntz, S. Tischer and O. Deutschmann, Urea derived deposits in diesel exhaust gas after-treatment: Integration of urea decomposition kinetics into a CFD simulation, *Chem. Eng. Sci.*, 2020, **211**, 115319.

23 P. M. Schaber, J. Colson, S. Higgins, D. Thielen, B. Anspach and J. Brauer, Thermal decomposition (pyrolysis) of urea in an open reaction vessel, *Thermochim. Acta*, 2004, **424**, 131–142.

24 M. Börnhorst, S. Langheck, H. Weickenmeier, C. Dem, R. Suntz and O. Deutschmann, Characterization of solid deposits from urea water solution injected into a hot gas test rig, *Chem. Eng. J.*, 2019, **377**, 119855.
25 W. Brack, B. Heine, F. Birkhold, M. Kruse and O. Deutschmann, Formation of Urea-Based Deposits in an Exhaust System: Numerical Predictions and Experimental Observations on a Hot Gas Test Bench, *Emiss. Control Sci. Technol.*, 2016, **2**, 115–123.
26 M. Börnhorst, *Dissertation*, KIT, 2019.
27 A. M. Bernhard, D. Peitz, M. Elsener, A. Wokaun and O. Kröcher, Hydrolysis and thermolysis of urea and its decomposition byproducts biuret, cyanuric acid and melamine over anatase TiO2, *Appl. Catal., B*, 2012, **115–116**, 129–137.
28 M. Koebel and E. O. Strutz, Thermal and Hydrolytic Decomposition of Urea for Automotive Selective Catalytic Reduction Systems: Thermochemical and Practical Aspects, *Ind. Eng. Chem. Res.*, 2003, **42**, 2093–2100.
29 M. Goldbach, A. Roppertz, P. Langenfeld, M. Wackerhagen, S. Füger and S. Kureti, Urea Decomposition in Selective Catalytic Reduction on V 2 O 5 /WO 3 /TiO 2 Catalyst in Diesel Exhaust, *Chem. Eng. Technol.*, 2017, **40**, 2035–2043.
30 M. Matsuoka, T. Kitamura, A. Obuchi, J. Tsuchida, K. Tanaka and M. Konno, Kinetic Measurements of HNCO Hydrolysis over SCR Catalyst, *International Powertrains, Fuels & Lubricants Meeting*, Heidelberg, Germany, September 17, 2018, DOI: 10.4271/2018-01-1764.
31 G. Piazzesi, M. Devadas, O. Kröcher, M. Elsener and A. Wokaun, Isocyanic acid hydrolysis over Fe-ZSM5 in urea-SCR, *Catal. Commun.*, 2006, **7**, 600–603.
32 European Commission, *European vehicle emissions standards – Euro 7 for cars, vans, lorries and buses*, https://ec.europa.eu/info/law/better-regulation/have-your-say/initiatives/12313-European-vehicle-emissions-standards-Euro-7-for-cars-vans-lorries-and-buses_en, (accessed 25.09.25).
33 US EPA, Amendments Related to Tier 3 Motor Vehicle Emission and Fuel Standards, Nonroad Engine and Equipment Programs, and MARPOL Annex VI Implementation | US EPA, https://www.epa.gov/regulations-emissions-vehicles-and-engines/amendments-related-tier-3-motor-vehicle-emission-and, (accessed 25.09.25).
34 K. Reif, *Dieselmotor-Management*, Springer Fachmedien Wiesbaden, Wiesbaden, 2020.
35 S. Tomin, K. Keller, U. Wagner, P. Lott, T. Koch and O. Deutschmann, Innovative engine test bench set-up for testing of exhaust gas aftertreatment and detailed gas species analysis for CNG-SI-operation, *Automot. Eng. Technol.*, 2024, **9**, 2.
36 G. Emig, E. Klemm and H. Freund, *Chemische Reaktionstechnik*, Springer Vieweg, Berlin, Heidelberg, 7th edn, 2024.
37 H. Gossler, B. L. Kee, H. Zhu, M. Hettel, O. Deutschmann and R. J. Kee, Flow and pressure characteristics in rectangular channels with internal cylindrical bodies, *Chem. Eng. Sci.*, 2016, **149**, 296–305.
38 R. Sala, J. Dzida and J. Krasowski, Ammonia Concentration Distribution Measurements on Selective Catalytic Reduction Catalysts, *Catalysts*, 2018, **8**, 231.
39 K. Lu, D. Liu, Y. Wu, S. Liu and S. Bai, A study on the high-efficiency mixer of the SCR system, *Mech. Ind.*, 2021, **22**, 7.
40 Z. Xu, J. Liu and J. Fu, Experimental investigation on the urea injection and mixing module for improving the performance of urea-SCR in diesel engines, *Can. J. Chem. Eng.*, 2018, **96**, 1417–1429.